On the Development of an Implicit High-Order Discontinuous Galerkin Solver for a Hybrid RANS-LES Model

F. Bassi, L. Botti, A. Colombo, A. Ghidoni, F. Massa and G. Noventa

1 Introduction

Recent years have seen an ever-increasing interest in turbulence models able to go beyond the limited predictive capability of the Reynolds-averaged Navier–Stokes (RANS) formulation. In the range of moderate Reynolds numbers, availability of large HPC resources now allows to employ Large Eddy Simulation (LES) also in complex flow applications. In this context, the practice of an implicit LES (ILES) based on the Discontinuous Galerkin (DG) method showed to be very promising due to the good dispersion and dissipation properties of DG methods. However, to date, characteristic Reynolds numbers of many industrial applications are too large for a fully resolved LES. For these applications the use of a hybrid RANS-LES model or a wall modelled LES approach seems mandatory. In hybrid RANS-LES models the RANS equations are active close to solid walls, where LES would be

F. Bassi · L. Botti · A. Colombo (✉) · F. Massa
Dipartimento di Ingegneria e Scienze Applicate, Università degli Studi di Bergamo, Dalmine, (BG), Italy
e-mail: alessandro.colombo@unibg.it

F. Bassi
e-mail: francesco.bassi@unibg.it

L. Botti
e-mail: lorenzo.botti@unibg.it

F. Massa
e-mail: francescocarlo.massa@unibg.it

A. Ghidoni · G. Noventa
Dipartimento di Ingegneria Meccanica e Industriale, Università degli Studi di Brescia, Brescia, Italy
e-mail: antonio.ghidoni@unibs.it

G. Noventa
e-mail: gianmaria.noventa@unibs.it

M. V. Salvetti et al. (eds.), *Direct and Large-Eddy Simulation XI*,
ERCOFTAC Series 25, https://doi.org/10.1007/978-3-030-04915-7_11

prohibitively costly, while LES is used in regions of separated flow where larger eddies can be resolved. Among the hybrid approaches available in the literature, we chose the eXtra-Large Eddy Simulation (X-LES) [1, 2] for three attractive features: (i) independence from the wall distance; (ii) use in LES mode of a clearly defined subgrid-scale (SGS) model [3]; (iii) use of the k-ω turbulence model integrated to the wall.

2 Implementation and Discretization of the X-LES Model

In this section we review some details of the proposed X-LES model implementation and DG discretization [2]. For the sake of compactness we only report the governing equations for the turbulent kinetic energy k and the logarithm of the specific dissipation rate $\widetilde{\omega}$

$$\frac{\partial}{\partial t}(\rho k) + \frac{\partial}{\partial x_j}\left(\rho u_j k\right) = \frac{\partial}{\partial x_j}\left[\left(\mu + \sigma^* \bar{\mu}_t\right)\frac{\partial k}{\partial x_j}\right] + P_k - D_k, \tag{1}$$

$$\frac{\partial}{\partial t}(\rho\widetilde{\omega}) + \frac{\partial}{\partial x_j}\left(\rho u_j \widetilde{\omega}\right) = \frac{\partial}{\partial x_j}\left[\left(\mu + \sigma \bar{\mu}_t\right)\frac{\partial \widetilde{\omega}}{\partial x_j}\right] + \left(\mu + \sigma\bar{\mu}_t\right)\frac{\partial\widetilde{\omega}}{\partial x_k}\frac{\partial\widetilde{\omega}}{\partial x_k} + P_\omega - D_\omega + C_D, \tag{2}$$

where the production, destruction and cross diffusion terms are

$$P_k = \tau_{ij}\frac{\partial u_i}{\partial x_j}, \quad P_\omega = \alpha\left[\alpha^*\frac{\rho}{e^{\widetilde{\omega}_r}}\left(S_{ij} - \frac{1}{3}\frac{\partial u_k}{\partial x_k}\delta_{ij}\right) - \frac{2}{3}\rho\delta_{ij}\right]\frac{\partial u_i}{\partial x_j}, \tag{3}$$

$$D_k = \beta^*\rho\bar{k}\hat{\omega}, \quad D_\omega = \beta\rho e^{\widetilde{\omega}_r}, \quad C_D = \sigma_d\frac{\rho}{e^{\widetilde{\omega}_r}}\max\left(\frac{\partial k}{\partial x_k}\frac{\partial\widetilde{\omega}}{\partial x_k}, 0\right), \tag{4}$$

and

$$\bar{\mu}_t = \alpha^*\frac{\rho\bar{k}}{\hat{\omega}}, \quad \bar{k} = \max\left(0, k\right). \tag{5}$$

In our implementation, being k limited to zero, X-LES actually switches between three different flow models, i.e., ILES, LES with a well defined explicit SGS model [3] and RANS closed by the k-ω model. The automatic switching among the models is obtained through the definition of a "composite" specific dissipation rate

$$\hat{\omega} = \max\left(e^{\widetilde{\omega}_r}, \frac{\sqrt{\bar{k}}}{C_1\Delta}\right), \tag{6}$$

where Δ is the SGS filter width and $C_1 = 0.05$. Although in the literature the filter width parameter is often related to the local mesh spacing, here we set Δ to a constant value over the whole computational grid.

The variable $\widetilde{\omega}_r$ in the source terms of Eqs. 3 and 4, and in the "composite" specific dissipation rate definition in Eq. 6, indicates that $\widetilde{\omega}$ must fulfill a suitably defined "realizability" condition, which sets a lower bound on $\widetilde{\omega}$. This constraint ensures that X-LES, regardless of being in RANS or LES mode, predicts positive normal turbulent stresses and satisfies the Schwarz inequality for shear stresses

$$\overline{\rho u_i'^2} \geq 0, \quad i = 1, 2, 3; \qquad \left(\overline{\rho u_i' u_j'}\right)^2 \leq \overline{\rho u_i'^2}\,\overline{\rho u_j'^2}, \quad i, j = 1, 2, 3, \quad i \neq j, \tag{7}$$

where u_i' indicates the fluctuating part of the ith component of the velocity and the overline symbol the temporal average operator.

Being in X-LES both the Reynolds and the subgrid stress tensor modelled according to the Boussinesq hypothesis, an overall "realizability" condition can be enforced through the definition of a suitably modified specific dissipation rate. In fact, after some algebra, Eqs. 7 can be written in terms of modelled stresses as

$$\frac{e^{\widetilde{\omega}}}{\alpha^*} - 3\left(S_{ii} - \frac{1}{3}\frac{\partial u_k}{\partial x_k}\right) \geq 0, \quad i = 1, 2, 3, \tag{8}$$

$$\begin{aligned} &\left(\frac{e^{\widetilde{\omega}}}{\alpha^*}\right)^2 - 3\left(S_{ii} + S_{jj} - \frac{1}{3}\frac{\partial u_k}{\partial x_k}\right)\frac{e^{\widetilde{\omega}}}{\alpha^*} \\ &+ 9\left[\left(S_{ii} - \frac{1}{3}\frac{\partial u_k}{\partial x_k}\right)\left(S_{jj} - \frac{1}{3}\frac{\partial u_k}{\partial x_k}\right) - S_{ij}^2\right] \geq 0, \quad i, j = 1, 2, 3, \quad i \neq j. \end{aligned} \tag{9}$$

Let us denote with a the maximum value of the unknown $e^{\widetilde{\omega}}/\alpha^*$ that fulfills the inequalities Eqs. 8 and 9. The lower bound $\widetilde{\omega}_{r0}$ that guarantees realizable stresses is then given by

$$\frac{e^{\widetilde{\omega}_{r0}}}{\alpha^*} = a. \tag{10}$$

Since in this work the underlaying turbulence model is the high-Reynolds version of k-ω, α^* is constant and the solution of Eq. 10 is trivial. The "realizability" constraint can be finally enforced as

$$\widetilde{\omega}_r = \max\left(\widetilde{\omega}, \widetilde{\omega}_{r0}\right). \tag{11}$$

X-LES equations are here discretized in space according to the DG method, see [2] for details. The complete governing system can be written in compact form as

$$\mathbf{P}\left(\mathbf{w}\right)\frac{\partial \mathbf{w}}{\partial t} + \nabla \cdot \mathbf{F}_{\mathrm{c}}\left(\mathbf{w}\right) + \nabla \cdot \mathbf{F}_{\mathrm{v}}\left(\mathbf{w}, \nabla \mathbf{w}\right) + \mathbf{s}\left(\mathbf{w}, \nabla \mathbf{w}\right) = \mathbf{0}, \tag{12}$$

where $\mathbf{w}$ is the unknown solution vector of the m variables, the tensors $\mathbf{F}_c$ and $\mathbf{F}_v$ are the convective and viscous flux functions, $\mathbf{s}$ is the vector of source terms. In this work we rely on the set of variables $\mathbf{w} = [\widetilde{p}, \widetilde{T}, u_i, k, \widetilde{\omega}]^T$, where $\widetilde{p} = \log(p)$ and $\widetilde{T} = \log(T)$. In practice we substitute (p, T) with $e^{\widetilde{p}}, e^{\widetilde{T}}$ in the governing equations, and use the polynomial approximation of the working variables $\widetilde{p}$ and $\widetilde{T}$ instead of p and T directly. This trick ensured, by design, the positivity of the thermodynamic unknowns at a discrete level, adding robustness to high-order simulations of transonic flows. The matrix $\mathbf{P}(\mathbf{w})$ is the transformation matrix that takes into account of the change of variables from the conservative set $\mathbf{w}_c = [\rho, \rho E, \rho u_i, \rho k, \rho\widetilde{\omega}]^T$ to the set $\mathbf{w}$.

The system of Eq. 12 is discretized in space firstly multiplying by an arbitrary smooth test function and then integrating by parts, thus obtaining its weak form. The solution and the test function are then replaced with a finite element approximation and a discrete test function both belonging to the set $\mathbf{V}_h := [\mathbb{P}_d^k(\mathscr{T}_h)]^m$, where $\mathbb{P}_d^k(\mathscr{T}_h) := \{v_h \in L^2(\Omega) \mid v_{h|K} \in \mathbb{P}_d^k(K),\ \forall K \in \mathscr{T}_h\}$ is the discrete polynomial space in physical coordinates. $\mathbb{P}_d^k(K)$ denotes the restriction of the polynomial functions of $d = 3$ variables and total degree k to the element K belonging to the triangulation $\mathscr{T}_h = \{K\}$, consisting of a set of non-overlapping elements, built on an approximation Ω_h of the computational domain Ω. A set of hierarchical and orthonormal basis functions for the space $\mathbb{P}_d^k(K)$ is computed following the approach of Bassi et al. [4].

Being the functional approximation discontinuous, the flux functions are not uniquely defined over the mesh faces, and thus a numerical flux vector is suitably defined both for the convective and viscous part of the equations. The former relies on the van Leer flux vector splitting method as modified by Hänel et al. [5]. The latter employs the BR2 scheme, proposed in Bassi et al. [6].

By assembling together all the elemental contributions a system of ordinary differential equations governing the evolution in time of the discrete solution is obtained. The accurate high-order time integration is performed by means of the multi-stage linearly implicit (Rosenbrock-type) Runge–Kutta schemes. Such schemes require the solution of a linear system at each stage, while the Jacobian matrix needs to be assembled only once per time step. An extended review of several Rosenbrock schemes as well as their coefficients is reported in [7].

3 Numerical Experiments

In this section we present preliminary results obtained with X-LES in the computation of the transonic turbulent flow through the NASA Rotor 37. These results are compared with the RANS simulations to assess the predicting capabilities of the two different approaches. This test case has been thoroughly investigated both numerically and experimentally, e.g. [8–10].

We performed all the computations up to $\mathbb{P}^2$ solution on a grid of 160512 20-node hexahedral elements (quadratic edges), created by agglomerating a structured linear mesh. The height of elements adjacent to the solid wall corresponds to $y^+ \approx 7$. The

governing equations were formulated in the non-inertial reference frame, see [10], setting the rotational speed equal to $\omega = [1800\text{rad/s}, 0, 0]^T$. We prescribed adiabatic wall boundary conditions on the blade, the hub and the tip surfaces. The total pressure and temperature, the flow angle $\alpha_1 = 0°$ and the turbulence intensity $Tu_1 = 3\%$ were set at the inlet, while the static pressure was imposed at the outlet. For the RANS computations we relied on the DG implementation proposed in [10, 11], performing the implicit time integration to the steady state by means of the linearized backward Euler scheme coupled with a pseudo-transient continuation strategy to evolve the CFL number. X-LES computations were initialized with the RANS fields, advancing the solution in time with the linearly-implicit third-order three-stages ROS3P Rosenbrock scheme [7, 12]. The X-LES filter width was set equal to $\Delta = 5 \times 10^{-5}$.

Figures 1 and 2 compare the RANS and instantaneous X-LES solutions in terms of pressure contours and skin friction lines on the blade. The unsteady nature of X-LES can be clearly appreciated together with the remarkably different distribution of separation lines with respect to the RANS result. In Figs. 3 and 4 the pitch-wise mass averaged $p_{0,2}/p_{0,1}$ and $T_{0,2}/T_{0,1}$ radial distributions for the RANS and X-LES computations are compared with the experimental data at 98% of the choked mass flow. X-LES results are averaged over 46800 time-steps, corresponding to 13 convective time units, defined as $t_c = c/(a\, M_{r,tip})$, where c is the chord at midspan, $M_{r,tip}$ the relative tip Mach number at the inlet, and a the speed of sound at the

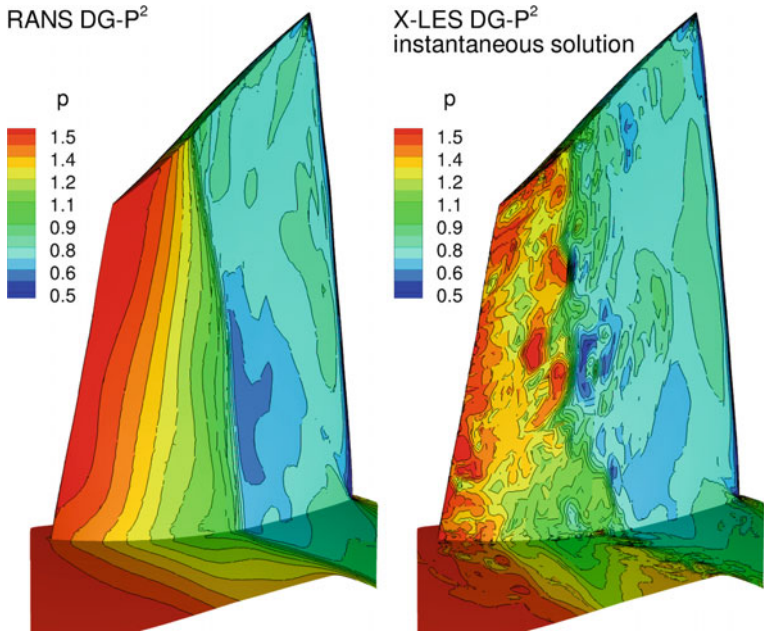

Fig. 1 Pressure contours, $\mathbb{P}^2$ solutions

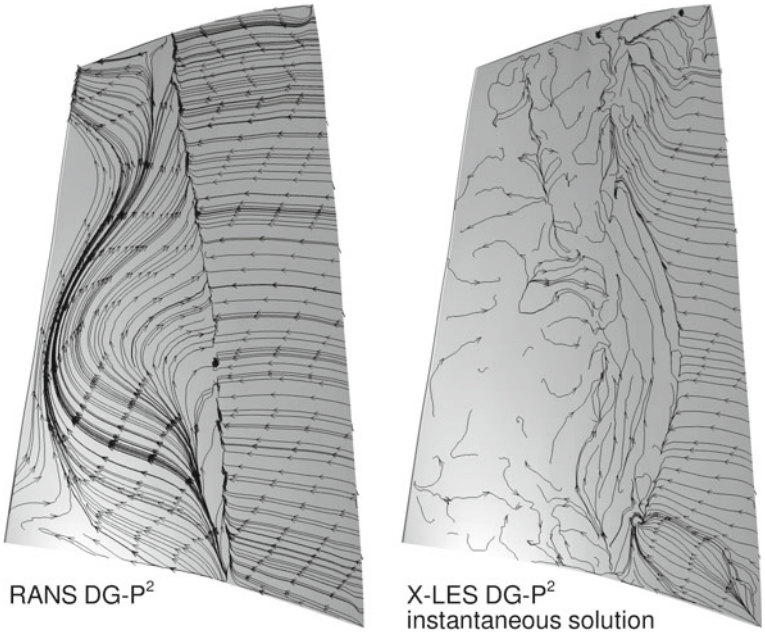

Fig. 2 Skin friction lines, $\mathbb{P}^2$ solutions

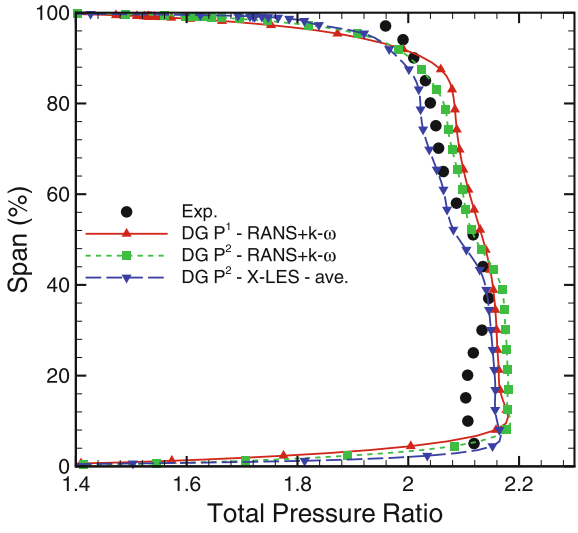

Fig. 3 Pitch-wise total pressure ratio $p_{0,2}/p_{0,1}$, $\mathbb{P}^{1\to 2}$ solutions

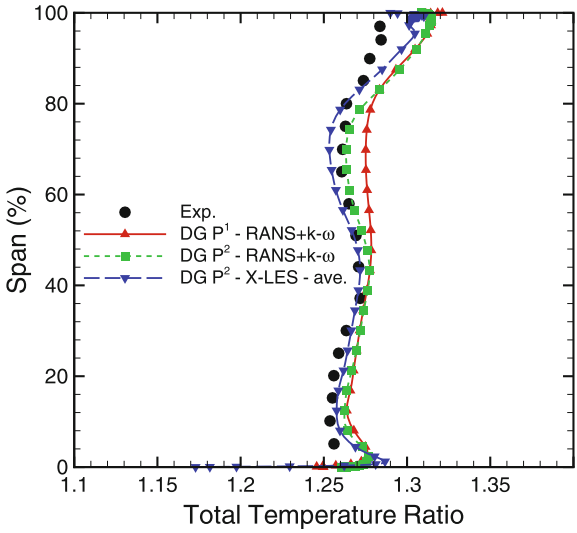

Fig. 4 Pitch-wise total temperature ratio $T_{0,2}/T_{0,1}$, $\mathbb{P}^{1\to 2}$ solutions

inlet. The pressure ratio distribution is better predicted by X-LES starting from 40% of the span, while up to 40% both models, i.e. RANS and X-LES, are not able to capture the total pressure deficiency. The total temperature distribution is better predicted by X-LES everywhere with the exception of the zone near 60% of the span, where it is slightly underestimated. At hub and tip regions some discrepancies with respect to experimental measurements occur, even if less pronounced for the X-LES; however similar behaviours are also observed for other numerical results reported in the literature.

4 Conclusion

A high-order DG method coupled with an implicit time integration strategy for the high-fidelity simulation of turbulent flows was presented. The X-LES hybrid approach was chosen, being considered appealing for many industrial applications characterized by high Reynolds numbers. X-LES proved to be robust and able to correctly deal with separated flows, also improving the predicting capabilities over RANS model.

Future work will be addressed to further investigate the filter width influence on results accuracy, to move towards very-large scale parallel computations (ten-of-thousands cores), and to include in our X-LES implementation some recently proposed improvements to the model [13].

Acknowledgements The results reported in this paper have been achieved using the PRACE Research Infrastructure resource MARCONI-KNL based at CINECA, Casalecchio di Reno, Italy, within the Project "Discontinuous Galerkin method for the X-LES of TRAnsonic flows" (DGX-TRA).

References

1. Kok, J.C., Dol, H.S., Oskam, B., van der Ven, H.: Extra-large eddy simulation of massively separated flows. AIAA Paper 2004–264 (2004)
2. Bassi, F., Botti, L., Colombo, A., Crivellini, A., Ghidoni, A., Nigro, A., Rebay, S.: Time Integration in the Discontinuous Galerkin Code MIGALE - Unsteady Problems. In: Kroll, N., Hirsch, C., Bassi, F., Johnston, C., Hillewaert, K. (eds.) IDIHOM: Industrialization of High-Order Methods - A Top-Down Approach. Notes on Numerical Fluid Mechanics and Multidisciplinary Design, vol. 128, pp. 205–230. Springer International Publishing, Berlin (2015)
3. Yoshizawa, A.: Statistical theory for compressible turbulent shear flows, with the application to subgrid modelling. Phys. Fluids **29**, 2152–2160 (1986)
4. Bassi, F., Botti, L., Colombo, A., Di Pietro, D., Tesini, P.: On the flexibility of agglomeration based physical space discontinuous Galerkin discretizations. J. Comput. Phys. **231**(1), 45–65 (2012). https://doi.org/10.1016/j.jcp.2011.08.018
5. Hänel, D., Schwane, R., Seider, G.: On the accuracy of upwind schemes for the solution of the Navier–Stokes equations, AIAA Paper 87-1105 CP. In: AIAA, Proceedings of the AIAA 8th Computational Fluid Dynamics Conference (1987)
6. Bassi, F., Rebay, S., Mariotti, G., Pedinotti, S., Savini, M.: A high-order accurate discontinuous finite element method for inviscid and viscous turbomachinery flows. In: Decuypere, R., Dibelius, G. (eds.) 2nd European Conference on Turbomachinery Fluid Dynamics and Thermodynamics, pp. 99–108. Technologisch Instituut, Antwerpen, Belgium (1997)
7. Bassi, F., Botti, L., Colombo, A., Ghidoni, A., Massa, F.: Linearly implicit Rosenbrock-type Runge–Kutta schemes applied to the discontinuous Galerkin solution of compressible and incompressible unsteady flows. Comput. Fluids **118**, 305–320 (2015)
8. Dunham, J.: CFD validation for propulsion system components. Technical Report AR-355. AGARD (1994)
9. Denton, J.D.: Lessons from Rotor 37. J. Thermal Sci. **6**, 1–13 (1997)
10. Bassi, F., Botti, L., Colombo, A., Crivellini, A., Franchina, N., Ghidoni, A.: Assessment of a high-order accurate Discontinuous Galerkin method for turbomachinery flows. Int. J. Comput. Fluid Dyn. **30**, 307–328 (2016). https://doi.org/10.1080/10618562.2016.1198783
11. Bassi, F., Crivellini, A., Rebay, S., Savini, M.: Discontinuous Galerkin solution of the Reynolds-Averaged Navier–Stokes and k-ω turbulence model equations. Comput. Fluids **34**, 507–540 (2005)
12. Lang, J., Verwer, J.: ROS3P–An accurate third-order Rosenbrock solver designed for parabolic problems. BIT **41**, 731–738 (2001)
13. Kok, J.C.: A stochastic backscatter model for grey-area mitigation in detached eddy simulations. Flow, Turbul. Combust. (2017). https://doi.org/10.1007/s10494-017-9809-y